

Short-range B -site ordering in the inverse spinel ferrite NiFe_2O_4 V. G. Ivanov,¹ M. V. Abrashev,¹ M. N. Iliev,² M. M. Gospodinov,³ J. Meen,² and M. I. Aroyo⁴¹*Faculty of Physics, University of Sofia, 1164 Sofia, Bulgaria*²*Texas Center for Superconductivity and Department of Physics, University of Houston, Houston, Texas 77204-5002, USA*³*Institute of Solid State Physics, Bulgarian Academy of Sciences, 1184 Sofia, Bulgaria*⁴*Departamento de Física de la Materia Condensada, Universidad del País Vasco, 48080 Bilbao, Spain*

(Received 4 May 2010; published 15 July 2010)

The Raman spectra of single crystals of NiFe_2O_4 were studied in various scattering configurations in close comparison with the corresponding spectra of $\text{Ni}_{0.7}\text{Zn}_{0.3}\text{Fe}_2\text{O}_4$ and Fe_3O_4 . The number of experimentally observed Raman modes exceeds significantly that expected for a normal spinel structure and the polarization properties of most of the Raman lines provide evidence for a microscopic symmetry lower than that given by the $Fd\bar{3}m$ space group. We argue that the experimental results can be explained by considering the short-range 1:1 ordering of Ni^{2+} and Fe^{3+} at the B sites of inverse spinel structure, most probably of tetragonal $P4_122/P4_322$ symmetry.

DOI: 10.1103/PhysRevB.82.024104

PACS number(s): 78.30.-j, 63.20.D-, 75.47.Lx

I. INTRODUCTION

The spinel ferrites with general formula $A\text{Fe}_2\text{O}_4$ have interesting physical properties and are of technology importance.¹ In particular, NiFe_2O_4 is of increased interest as this material, in the form of bulk, powder, thin film, or nanoparticles, finds or promises numerous applications in magnetic storage systems,² magnetic-resonance imaging,³ spintronics,^{4,5} etc. At present it is accepted that NiFe_2O_4 crystallizes in inverse spinel structure,⁶⁻⁹ described by the face-centered-cubic (fcc) space group $Fd\bar{3}m$ (No. 227, $Z=8$). In this structure the tetrahedral A sites (8a) are occupied by half of the Fe^{3+} cations, whereas the rest of Fe^{3+} and Ni^{2+} cations are distributed over the octahedral B sites (16d). A fundamental question however arises whether Fe^{3+} and Ni^{2+} is spread in a random fashion among the B sites or exhibit specific short-range order on a spatial scale, which is below the detection limit of the standard diffraction techniques. This issue can be addressed effectively by polarization Raman spectroscopy since the number, the frequencies, and the polarization selection rules of the Raman-active vibrational modes are highly sensitive to the atomic short-range order. For the normal spinel structure only five Raman-allowed phonons ($A_{1g}+E_g+3F_{2g}$) are expected and this is the case for number of materials such as Co_3O_4 ,¹⁰ CdCr_2Se_4 ,¹¹ and Fe_3O_4 above the Verwey transition temperature,¹² to mention a few. Another group of spinels, such as NiFe_2O_4 ,^{13,14} NiAl_2O_4 ,¹⁵ and CoFe_2O_4 ,^{16,17} exhibit much richer Raman spectra with number of additional peaks. The latter materials are with inverse or partly inverse spinel structure and it is reasonable to assume that the appearance of additional Raman lines is somehow related to the presence of nonequivalent atoms at the B sites, which may have the following consequences for the Raman spectra: (i) the random distribution of inequivalent B' and B'' atoms destroys the translation symmetry, in particular of the oxygen sublattice, and activates otherwise forbidden phonon modes. One expects in this case additional broad Raman structures which roughly reproduce the smeared one-phonon density of states;¹⁸ and (ii) a short-range ordering of B' and B'' atoms may result in formation of

domains of symmetry lower than $Fd\bar{3}m$ with new sets of Raman-allowed phonons. The coexistence of twin variants of these local structures leads to a superposition of spectra corresponding to different scattering configurations.

In this work we report results of polarized Raman study of NiFe_2O_4 . The analysis is done in close comparison with lattice dynamics calculations for spinel structures with either full disorder or ordering of Ni^{2+} and Fe^{3+} at the B sites as well with the corresponding spectra of $\text{Ni}_{0.7}\text{Zn}_{0.3}\text{Fe}_2\text{O}_4$ and Fe_3O_4 . A conclusion is made that at a microscopic level the structure of NiFe_2O_4 can be considered as a mixture of twin variants of a structure with Fe^{3+} and Ni^{2+} ordered over the B sites.

II. SAMPLES AND METHODS

The first step in the growth of NiFe_2O_4 and $\text{Ni}_{0.7}\text{Zn}_{0.3}\text{Fe}_2\text{O}_4$ single crystals was sintering of polycrystalline samples by solid-state reaction of stoichiometric amounts of NiO , Fe_2O_3 , and ZnO annealed for 48 h at 1150 °C in oxygen atmosphere. As a next step the high-temperature solution growth method was applied using $\text{PbO-PbF}_2\text{-B}_2\text{O}_3$ flux with ratio of the components 0.50:0.48:0.02 for NiFe_2O_4 and 0.67:0.32:0.01 for $\text{Ni}_{0.7}\text{Zn}_{0.3}\text{Fe}_2\text{O}_4$, respectively. The flux was mixed with NiFe_2O_4 powder in a 10:1 ratio or with $\text{Ni}_{0.7}\text{Zn}_{0.3}\text{Fe}_2\text{O}_4$ in a 7:1 ratio and annealed in 500 ml platinum crucible at 1225 °C in air for 48 h. After annealing the temperature was decreased to 950 °C at a rate of 0.5 °C/h for NiFe_2O_4 and to 1000 °C at a rate of 1 °C/h for $\text{Ni}_{0.7}\text{Zn}_{0.3}\text{Fe}_2\text{O}_4$. The flux was decanted and the crystals of up to 5 mm in size were removed from the bottom of the Pt crucible. These crystals were of octahedral shape with large (111) and smaller (100) and (110) facets. The Fe_3O_4 sample was natural polycrystalline magnetite with typical grain size of 300 μm , large enough for obtaining polarized Raman spectra in exact scattering configuration from properly oriented microcrystal surfaces. The elemental content has been confirmed by x-ray wavelength dispersive spectrometry using a JEOL JXA8600 electron microprobe analyzer.

TABLE I. Raman polarization selection rules for the spinel $Fd\bar{3}m$ structure.

Mode	XX	X'X'	XY	X'Y'
A_{1g}	a^2	a^2	0	0
E_g	$4b^2$	b^2	0	$3b^2$
F_{2g}	0	d^2	d^2	0

The polarized Raman spectra were measured from (100) cubic surfaces with a triple T64000 spectrometer equipped with microscope. The spectra obtained with 633, 515, 488, or 458 nm excitation were practically the same.

III. RESULTS AND DISCUSSION

A. Polarized Raman spectra of $NiFe_2O_4$, Fe_3O_4 , and $Ni_{0.7}Zn_{0.3}Fe_2O_4$

From symmetry considerations one expects for the normal spinel $Fd\bar{3}m$ structure five ($A_{1g}+E_g+3F_{2g}$) Raman-active modes, which could be identified by measuring the Raman spectra in several exact scattering configurations, e.g., XX, XY, X'X', and X'Y', the first and second letters in these notations correspond, respectively, to the polarization of incident and scattered light, where X, Y, X', and Y' denote the $[100]_c$, $[010]_c$, $[110]_c$, and $[1\bar{1}0]_c$ cubic directions. As it follows from Table I, one expects two Raman lines ($A_{1g}+E_g$) in the XX spectrum, five lines ($A_{1g}+E_g+3F_{2g}$) in the X'X' spectrum, three ($3F_{2g}$) lines in the XY spectrum, and only one (E_g) line in the X'Y' spectrum.

In Fig. 1 are compared the experimental Raman spectra of $NiFe_2O_4$ and the closely related spinel Fe_3O_4 obtained at room temperature with 488 nm excitation. The spectra of $NiFe_2O_4$ taken with 633 nm excitation are shown in more detail in Fig. 2. The selection rules for the Raman bands of Fe_3O_4 follow strictly those for the normal spinel structure (see Table I). It is to be expected since the experimental temperature is well above the Verwey transition temperature of magnetite and, therefore, the charge is smeared uniformly among the Fe B sites. In contrast to Fe_3O_4 , the number of experimentally observed Raman lines in the spectra of $NiFe_2O_4$ exceeds significantly the number expected for a normal spinel structure and the polarization rules are strictly followed for only few lines, namely, those at $213\text{ cm}^{-1}(F_{2g})$, $333\text{ cm}^{-1}(E_g)$, and $705\text{ cm}^{-1}(A_{1g})$. It is remarkable, however, that these spectra are practically identical to those reported earlier for $NiFe_2O_4$ crystals, thin films, and nanocrystalline samples from different sources (see, e.g., Refs. 13 and 14). Much richer than expected Raman spectra have been also reported for other compounds, such as $NiAl_2O_4$, with nominally inverse spinel structure.¹⁵

The larger number of Raman-active modes in inverse spinels have been discussed before and has tentatively been explained in terms of defect-induced lattice distortions due to deviation from stoichiometry and/or coexistence of “normal” and “inverse” domains.^{13,15} It seems that the deviation from the stoichiometry has little effect on the Raman spectra. In

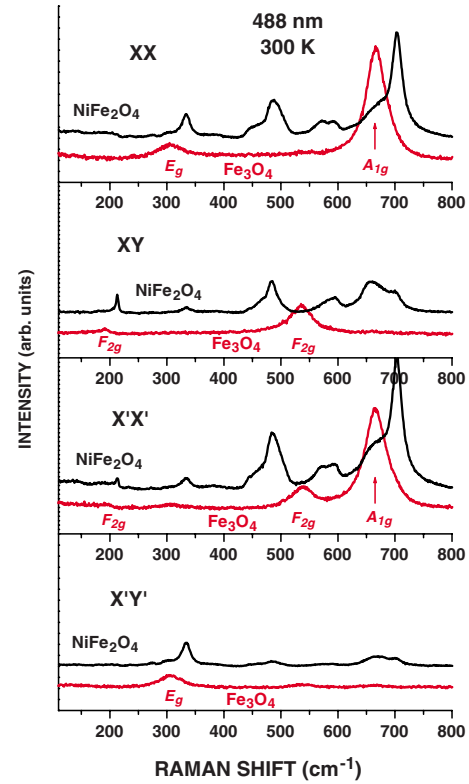


FIG. 1. (Color online) Polarized Raman spectra of $NiFe_2O_4$ and Fe_3O_4 as obtained at room temperature with 488 nm excitation.

Fig. 3 are compared the Raman spectra of $NiFe_2O_4$ and $Ni_{0.75}Zn_{0.25}Fe_2O_4$. The Zn^{2+} ion has a larger ionic radius than Ni^{2+} and is expected to increase the structural disorder of the oxygen sublattice. If the extra lines in the Raman spectra of $NiFe_2O_4$ were induced by a disorder, one would expect their relative intensity to increase in the Zn-substituted samples. In contrast, upon Zn substitution for Ni these lines broaden and

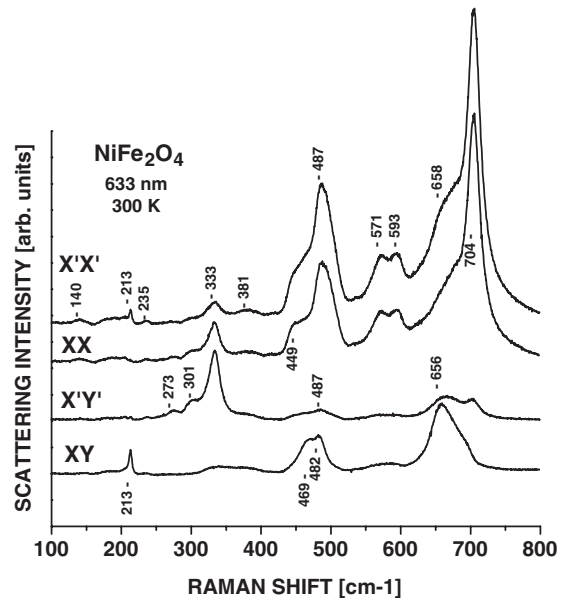


FIG. 2. Polarized Raman spectra of $NiFe_2O_4$ as obtained at room temperature with 633 nm excitation.

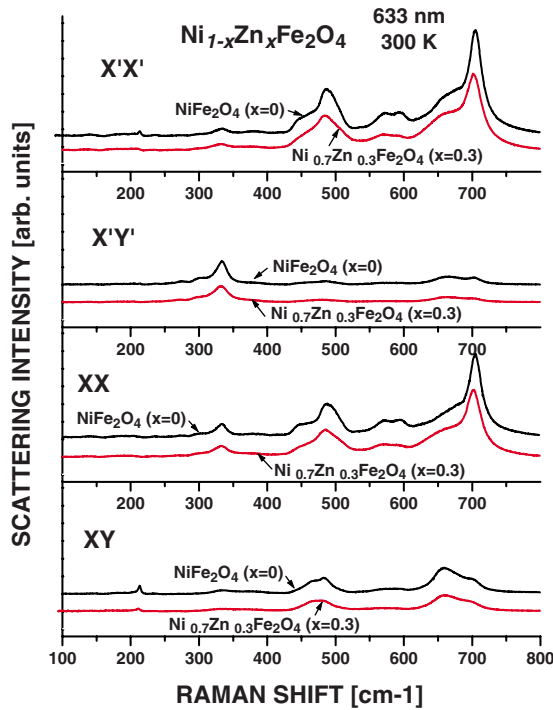


FIG. 3. (Color online) Polarized Raman spectra of NiFe_2O_4 and $\text{Ni}_{0.7}\text{Zn}_{0.3}\text{Fe}_2\text{O}_4$ as obtained at room temperature with 633 nm excitation.

decrease in intensity. Therefore, the additional lines in the Raman spectrum of NiFe_2O_4 indicate to a short-range order of Fe and Ni cations rather than a random distribution over the octahedral B positions.

B. Raman phonons in B site ordered phases in inverse spinels

1. Symmetry aspects of the 1:1 ordering at the B sites of inverse spinel structure

The symmetry aspects of the 1:1 ordering at the B sites of inverse spinel structure have been discussed in detail by Haas.¹⁹ It has been shown that there are two possible types of such ordering, α type and β type, illustrated in Fig. 4 and shortly described below.

The α -type order is characterized by $\cdots B''-B'-B''-B'-\cdots$ chains along the $[110]$ and $[1\bar{1}0]$ cubic directions. The space group is $P4_122$ (No. 91) with a tetragonal unit cell two times smaller than the face-centered spinel unit cell with lattice parameters $\vec{a}_t = \frac{1}{2}(\vec{a}_c + \vec{b}_c)$, $\vec{b}_t = \frac{1}{2}(\vec{a}_c - \vec{b}_c)$, and $\vec{c}_t = \vec{c}_c$. The same type of ordering can be described by the $P4_322$ (No. 95) space group, which is enantiomorphic to $P4_122$. The atomic site symmetries and the classification of the normal modes of vibration in the two space groups are equivalent. For this reason our further analysis will be done almost exclusively in the context of $P4_122$ group. From symmetry considerations the $Fd\bar{3}m$ - $P4_122/P4_322$ disorder-order transition is of first order. Therefore, in the phase diagram one expects two-phase region (miscibility gap) where the cubic and the tetragonal phases coexist. If upon cooling α -type ordering does take place, the tetragonal axis may be aligned along each of the

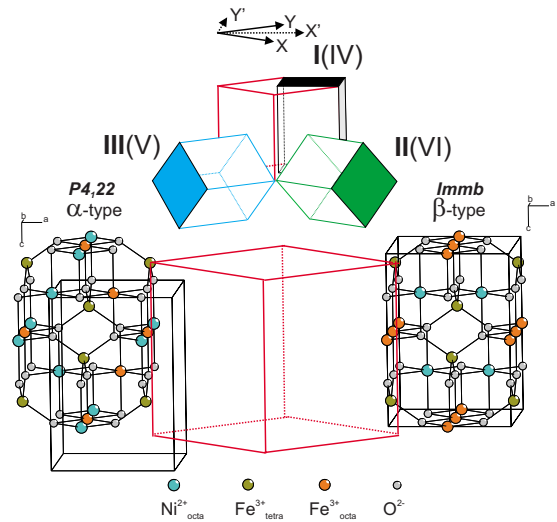


FIG. 4. (Color online) α -type ($P4_122/P4_322$) and β -type ($Imma$) ordering in inverse spinel structure. The orientation of the twin variants, I, II, and III for the tetragonal structure and IV, V, and VI for the orthorhombic structure, with respect to the cubic directions are also shown.

three equivalent \vec{a}_c , \vec{b}_c , or \vec{c}_c cubic directions. This implies that at a microscopic level six types of tetragonal domains, three types for $P4_122$, and three for $P4_322$, with mutually orthogonal fourfold axes may coexist at room temperature (Fig. 4). The enantiomorphic $P4_122/P4_322$ pairs of domains with the same orientation of the fourfold axis will be referred by a common number, I, II, and III for the cubic X , Y , and Z directions, respectively. In the case of domains of relatively small size (≤ 50 lattice constants), their presence will remain below the detection limits of standard diffraction techniques.

The β -type order is characterized by $\cdots B''-B'-B''-B'-\cdots$ chains along the $[110]$ direction and $\cdots B''-B''-B''-B''-\cdots$ chains along the $[1\bar{1}1]$ cubic directions (Fig. 4). The space group is $Imma$ (No. 74) with an orthorhombic unit cell two times smaller than the face-centered spinel unit cell [lattice parameters $\vec{a}_o = \frac{1}{2}(\vec{a}_c + \vec{b}_c)$, $\vec{b}_o = \frac{1}{2}(\vec{a}_c - \vec{b}_c)$, and $\vec{c}_o = \vec{c}_c$]. Here again the phase transition from spinel to orthorhombic structure is of first-order type and at a microscopic level three pairs (IV, V, and VI) of mutually orthogonal domains may coexist within the framework of an averaged spinel structure.

The experimentally confirmed averaged cubic structure of NiFe_2O_4 will be compatible with tetragonal $P4_122/P4_322$ and/or orthorhombic $Imma$ structure(s) if the twin variants of these structures are uniformly oriented with respect to the cubic axes as shown in Fig. 4. This means that the experimental Raman spectrum in a given cubic scattering configuration will be a superposition of spectra obtained simultaneously from tetragonal $P4_122$ twin variant in three different scattering configurations, corresponding to types (I), (II), or (III) orientation. The number of twin variants and, hence, the scattering configurations is doubled to six for the orthorhombic $Imma$ structure, accounting that a_o and b_o parameters are interchangeable.

Due to lower symmetry (compared to that of an ideal

TABLE II. Atomic site symmetries and corresponding Γ -point modes for the $Fd\bar{3}m$, $P4_122$, and $Imma$ structures of NiFe_2O_4 . For the ordered $P4_122$ and $Imma$ structures only Raman modes are shown.

$Fd\bar{3}m$ (cubic)			$P4_122$ (tetragonal)			$Imma$ (orthorhombic)		
Atom	Wyckoff index	Γ -point modes	Atom	Wyckoff index	Raman modes	Atom	Wyckoff index	Raman modes
Fe(1)	8a	$F_{2g}+F_{1u}$	Fe(1)	4c	$A_1+2B_1+B_2+3E$	Fe(1)	4e	$A_g+B_{2g}+B_{3g}$
Ni/Fe(2)	16d	$A_{2u}+E_u+F_{2u}+2F_{1u}$	Ni	4a	$A_1+B_1+2B_2+3E$	Ni	4c	
			Fe(2)	4b	$A_1+B_1+2B_2+3E$	Fe(2)	4b	
O	32e	$A_{1g}+A_{2u}+E_g+E_u+$ $F_{2u}+2F_{2g}+2F_{1u}+F_{1g}$	O(1)	8d	$3A_1+3B_1+3B_2+6E$	O(1)	8h	$2A_g+B_{1g}+B_{2g}+2B_{3g}$
			O(2)	8d	$3A_1+3B_1+3B_2+6E$	O(2)	8i	$2A_g+B_{1g}+2B_{2g}+B_{3g}$
Total Raman		$A_{1g}+E_g+3F_{2g}$	Total		$9A_1+10B_1+11B_2+21E$	Total		$5A_g+2B_{1g}+4B_{2g}+4B_{3g}$
1 acoustic +4 IR		$5F_{1u}$						
Inactive		$2A_{2u}+2E_u+2F_{2u}+F_{1g}$						

spinel) the number of Raman-allowed modes in B -site-ordered structures increases. Their classification is given in Table II. The polarization selection rules for the B -site-ordered $P4_122$ and $Imma$ structures, averaged over all twin variants, are summarized in Tables III and IV.

The tetragonal structure gives rise to 84 normal modes (accounting for the mode degeneracy), which is twice the

number of normal modes in the cubic structure. This is due to the fact that the primitive cell of $P4_122$ has two times bigger volume than the primitive cell of the fcc structure. By means of the group-subgroup relations half of the normal modes in the tetragonal structure can be mapped onto Γ -point modes of the cubic structure. For the Raman-active modes the correspondence is

TABLE III. Polarization selection rules for the scattering from $P4_122$ structures averaged over the three twin variants with I,II,- and III-type orientation with respect to the cubic axes.

Mode	Raman tensor	XX (cubic)	XY (cubic)	$X'X'$ (cubic)	$X'Y'$ (cubic)
A_1	$\begin{bmatrix} a & & \\ & a & \\ & & b \end{bmatrix}$	$\frac{2}{3}a^2 + \frac{1}{3}b^2$	0	$\frac{1}{3}a^2 + \frac{1}{6}(a+b)^2$	$\frac{1}{6}(a-b)^2$
B_1	$\begin{bmatrix} c & & \\ & -c & \\ & & \end{bmatrix}$	0	$\frac{1}{3}c^2$	$\frac{1}{3}c^2$	0
B_2	$\begin{bmatrix} & d & \\ d & & \\ & & \end{bmatrix}$	$\frac{2}{3}d^2$	0	$\frac{1}{6}d^2$	$\frac{1}{2}d^2$
E	$\begin{bmatrix} & & e \\ & e & \\ & & -e \\ -e & & \end{bmatrix}$	0	$\frac{2}{3}e^2$	$\frac{2}{3}e^2$	0

TABLE IV. Polarization selection rules for the scattering from *Imma* structures averaged over the six twin variants with I(IV)-,II(V),- and III(VI)-type orientation with respect to the cubic axes.

Mode	Tensor	XX (cubic)	XY (cubic)	$X'X'$ (cubic)	$X'Y'$ (cubic)
A_1	$\begin{bmatrix} a & & \\ & b & \\ & & c \end{bmatrix}$	$\frac{1}{6}(a+b)^2 + \frac{1}{3}c^2$	$\frac{1}{12}(a-b)^2$	$\frac{1}{6}a^2 + \frac{1}{6}b^2 + \frac{1}{24}(a+b+2c)^2$	$\frac{1}{24}(a+b-2c)^2$
B_{1g}	$\begin{bmatrix} & & d \\ & d & \\ & & \end{bmatrix}$	$\frac{2}{3}d^2$	0	$\frac{1}{6}d^2$	$\frac{1}{2}d^2$
B_{2g}	$\begin{bmatrix} & & e \\ & e & \\ & & \end{bmatrix}$	0	$\frac{1}{3}e^2$	$\frac{1}{3}e^2$	0
B_{3g}	$\begin{bmatrix} & & f \\ & f & \\ & & \end{bmatrix}$	0	$\frac{1}{3}f^2$	$\frac{1}{3}f^2$	0

$$A_{1g} \rightarrow A_1, \quad (1)$$

$$E_g/E_u \rightarrow A_1 + B_2, \quad (2)$$

$$F_{1g}/F_{1u} \rightarrow A_2 + E, \quad (3)$$

$$F_{2g}/F_{2u} \rightarrow B_1 + E. \quad (4)$$

The rest of the Γ -point modes of the tetragonal structure originate from a zone folding of the fcc Brillouin zone, which maps X^* , the star of zone-boundary X point of $Fd\bar{3}m$, onto Γ point of $P4_122$. Among the Raman-active modes of the tetragonal structure such are $5A_1 + 5B_1 + 8B_2 + 10E$. From a physical point of view the new spectral features in $P4_122$ can be considered as a result of splitting of the degenerated Raman modes of $Fd\bar{3}m$ into doublets, as well as activation of

the IR F_{1u} , Γ -point silent F_{1g} and F_{2u} , and zone-boundary modes.

The primitive cell volumes of the orthorhombic *Imma* structure and fcc structure are equal and no zone folding takes place. All Raman-active modes of the orthorhombic structure can be mapped onto Γ -point modes of $Fd\bar{3}m$,

$$A_{1g} \rightarrow A_g, \quad (5)$$

$$E_g \rightarrow A_g + B_{1g}, \quad (6)$$

$$F_{2g} \rightarrow A_g + B_{2g} + B_{3g}, \quad (7)$$

$$F_{1g} \rightarrow B_{1g} + B_{2g} + B_{3g}. \quad (8)$$

Therefore, the extra Raman bands in *Imma* should consist of a doublet originating from the E_g mode, three triplets origi-

TABLE V. Shell-model parameters for NiFe_2O_4 .

Atom	Core charge X	Shell charge Y	Core-shell spring constant k (eV/Å ²)
Ni	+2		
Fe	+3		
O	0.513	-2.513	72.53
Atomic pair	A (eV)	ρ (Å)	C (eV \times Å ⁶)
Ni core-O shell	681.9	0.337	0
Fe core-O shell	986.1	0.337	0
O shell-O shell	22764.0	0.149	27.879

TABLE VI. Calculated frequencies of the Raman-active modes in NiFe_2O_4 for the three structural models: B -site disorder of a macroscopic $Fd\bar{3}m$ symmetry, α -type ordering (symmetry $P4_122$), and β -type ordering (symmetry $Imma$).

$Fd\bar{3}m$			$P4_122$				$Imma$			
A_g	E_g	F_{2g}	A_1	B_1	B_2	E	A_g	B_{1g}	B_{2g}	B_{3g}
			168	148	155	147				
				171	205	207				
					235	235	227			229
		255	253	248		246		248		
						253			252	
						263				
	300		295		305	293				
				329	306	314				
				350	353	328			336	
			395	381	374	367	387			
				415		407				405
						438		438		
		465		465		464				
						469				
			498	498	496	490				
					516	514				
			573		574	556			588	
		618		612		615	605			613
			635	649	661	665	659		643	
687			694			718				689
							744			

nating from the F_{2g} modes, and a triplet resulting from activation of the silent F_{1g} mode of the fcc structure.

2. Lattice dynamics calculations of Γ -point Raman phonons of inverse spinel NiFe_2O_4

Theoretical results for the lattice dynamics of NiFe_2O_4 with either disorderly distributed or ordered Ni^{2+} and Fe^{3+} over the octahedral B sites were obtained by means of a shell model using the general utility lattice program.²⁰

In order to reduce the number of adjustable model parameters some approximations were applied. First, a valence shell was considered for the O atoms only while Ni and Fe were treated as rigid ions. Second, the van der Waals attractive interaction was considered to act only between O shells while it was neglected for the Ni (Fe) core-O shell pairs. These assumptions are justified by the much higher polarizability of the O^{2-} ion compared to that of the transition-metal ions. The rigid-ion approximation for transition metals is a common approximation in the shell-model calculations on transition-metal oxides.²¹ The short-range interatomic interactions were modeled by a Buckingham potential: $V(r) = A \exp(-r/\rho) - C/r^6$, where a nonzero van der Waals constant C was retained for the O shell-O shell pairs only.

The starting model parameters were taken from the widely utilized parameter set of Lewis and Catlow,²¹ with a

formal charge of +3 assigned to the Fe ions in both A and B positions. As a next step the Buckingham A parameters for the Ni^{2+} core-O shell and Fe^{3+} core-O shell pairs were optimized in order to reproduce the experimentally observed lattice parameters for NiFe_2O_4 , the cubic face-centered lattice constant $a_c = 8.337 \text{ \AA}$ and the fractional oxygen position $u = 0.831$. It was assumed at this stage that even if a cation ordering takes place in the B positions, on a macroscopic scale (above the detection limit of the diffraction techniques) the material can be described in a cubic approximation. For this reason the fit was performed by setting equal partial occupancies of 0.5 for the Fe^{3+} and Ni^{2+} ions in the B position of the ideal cubic $Fd\bar{3}m$ structure. This is equivalent to introduction of an ‘‘average’’ cation in B position having charge, mass, and short-range potential parameters, which are arithmetic means between those corresponding to Ni^{2+} and Fe^{3+} . The as obtained shell-model parameters are summarized in Table V. Finally, the set of fitted parameters was used to calculate the Γ -point normal modes for the average-atom cubic $Fd\bar{3}m$ structure, which are assumed to mimic the positions of the main Raman bands in the case of complete cation disorder at the B sites. The same parameters were utilized to optimize the lattice parameters of the ordered α - and β -type structures and to calculate the corresponding Γ -point modes. The calculated normal-mode frequencies for the three structural models are listed in Table VI.

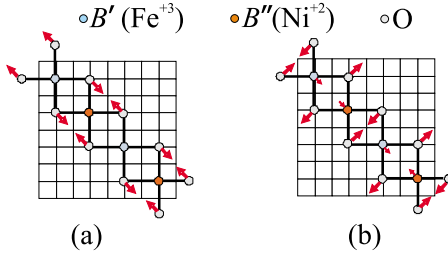


FIG. 5. (Color online) A $z=3/8$ cross section of the $Fd\bar{3}m$ unit cell. Two fcc zone-boundary normal modes, which split into A_1 - B_2 pairs upon α -type 1:1 arrangement at B positions: (a) 571–593 cm^{-1} and (b) 449–487 cm^{-1} .

3. Raman spectroscopy evidence for 1:1 ordering at the B sites of NiFe_2O_4

Unlike standard x-ray and neutron-diffraction techniques, which are most sensitive to the long-range order, the Raman scattering is more sensitive to the local short-range order, which may differ from the averaged long-range one. As discussed above, the 1:1 ordering at the B sites gives rise to structures of tetragonal $P4_122$ (No. 91) or orthorhombic $Immb$ (No. 74) symmetry.

As it follows from the polarization selection rules, the fully symmetrical modes $A_{1g}(Fd\bar{3}m)$, $A_1(P4_122)$, or $A_g(Imma)$ can be identified by their stronger intensity in the XX and $X'X'$ spectra compared to that in the XY and $X'Y'$ spectra. Such are the Raman peaks at 140, 235, 381, 449, 487, 571, 593, and 704 cm^{-1} . Their number exceeds the expected single A_{1g} mode for $Fd\bar{3}m$ or five A_g modes for $Imma$ structure. Therefore, it is plausible to accept that at least part of these peaks originate from α -type ordering at the octahedral sites, corresponding to local $P4_122$ structure. Indeed, these experimental frequencies show closest match with the following calculated frequencies of the A_1 modes in the $P4_122$ structure: 168, 253, 395, 498, 573, and 694 cm^{-1} . In the same time, the calculations show a large frequency gap between 387 and 605 cm^{-1} in the A_g channel of the $Imma$ structure, which makes the β -type ordering unlikely from a spectroscopic point of view.

It is instructive to comment on the experimentally observed splitting of the intense band around 580 cm^{-1} into two components at 571 and 593 cm^{-1} . According to our calculations there are two closely separated modes in the $P4_122$ structure at 573 and 574 cm^{-1} of A_1 and B_2 symmetries, respectively. The selection rules for the tetragonal structure (see Table III) predict the B_2 modes to appear in the same scattering configuration as A_1 modes. Thus the experimentally observed components can be assigned to an A_1 - B_2 pair. The inspection of the atomic displacement pattern in these modes shows that they can be mapped to a doubly degenerated X -point zone-boundary mode of the cubic structure, which becomes a Raman-active Γ -point mode in the $P4_122$ structure due to zone folding [see Fig. 5(a)]. Similarly, the 449 and 487 cm^{-1} bands can be ascribed to another A_1 - B_2 pair originating from the fcc zone-boundary X point [see Fig. 5(b)]. In a cubic structure the B' and B'' sites are equivalent and the double degeneracy of each of these modes results

from the fact that depending on the choice of the BO_2 chains the oxygen atoms can vibrate in two independent directions, e.g., $[110]_c$ and $[011]_c$ while the vibration in the third symmetry-equivalent direction $[101]_c$ is a linear superposition of the other two vibrations.

Additional pieces of evidence for the presence of tetragonal α -type ordering could be drawn from an analysis of the other scattering configurations. The mode at 213 cm^{-1} is active in $X'X'$ and XY configurations and could be assigned to F_{2g} , B_1+E , or $A_g+B_{2g}+B_{3g}$ vibrations in the cubic, tetragonal, and orthorhombic structures, respectively. Again, the best correspondence is found with the E mode at 208 cm^{-1} for the $P4_122$ structure. However, taking into account the unavoidable uncertainty of calculations, the B_{2g} mode at 229 cm^{-1} of the $Imma$ structure is also a like candidate for that spectral feature.

The cubic E_g channel includes the XX , $X'X'$, and $X'Y'$ scattering configurations with a smallest expected intensity in the $X'X'$ configuration. Similar selection rules are expected for the A_1+B_2 modes in the $P4_122$ structure and the A_g+B_{1g} modes in the $Imma$ structure. The experimentally detected modes at 273, 301, and 333 cm^{-1} follow closely these selection rules. The multiplicity of the observed frequencies suggests the presence of ordered structures since one single E_g mode is expected for the cubic structure. Most likely, the experimentally observed spectral bands correspond to the A_1 and B_2 modes of the $P4_122$ structure, whose calculated frequencies fall in the range 295–353 cm^{-1} (see Table VI). Since the frequency splitting between some of the modes (305–306 and 350–353 cm^{-1}) is comparable to the spectrometer resolution, experimentally they may appear as single spectral features leading to only three observable frequencies. It is worthy to mention that according to our calculations no A_g or B_{1g} modes are expected in this frequency range for the $Imma$ structure.

Finally, the band at 656–658 cm^{-1} is active in all scattering configurations. According to Table IV such a behavior is expected for the A_g modes of the orthorhombic $Imma$ structure. One plausible explanation of this feature is the calculated A_g mode at 659 cm^{-1} . Alternatively, a doublet of closely separated modes of B_2 symmetry at 660.7 cm^{-1} and of E symmetry at 665.4 cm^{-1} is predicted for the tetragonal $P4_122$ structure. Due to their similar frequencies the two modes may be indistinguishable experimentally and should appear in all scattering configuration (Table III).

IV. SUMMARY AND CONCLUSIONS

We present detailed polarization Raman measurements of the inverse spinel NiFe_2O_4 . The number and the polarization selection rules for the observed Raman bands do not support the model of stochastic distribution of Ni^{2+} and Fe^{3+} cations among the octahedral B sites.

By using symmetry analysis and shell-model lattice dynamics calculations we examined the experimental data against two models of B site 1:1 ordering, α type of tetragonal $P4_122/P4_322$ symmetry and β type of orthorhombic $Imma$ symmetry. All experimental Raman bands are consistent by symmetry and frequency with the calculated normal

modes of the α -type structure, The β -type ordering can explain only part of the observed bands.

On the basis of the above arguments we can conclude that Ni^{2+} and Fe^{3+} exhibit 1:1 ordering at the octahedral sites of NiFe_2O_4 , most probably of tetragonal $P4_122/P4_322$ symmetry. However, the *Imma* structure cannot be definitively ruled out due to the good correspondence of some calculated frequencies to experimentally observed bands. It is possible that the two types of ordering coexist with prevalence of the tetragonal structures. Macroscopically the material exhibits cu-

bic symmetry due to the presence of randomly oriented twin variants of the ordered structures.

ACKNOWLEDGMENTS

This work is supported in part by the State of Texas through The Texas Center for Superconductivity at the University of Houston and partly by Contracts No. DO 02-167/2008 and No. TK-X-1712/2007 of the Bulgarian National Scientific Research Fund.

-
- ¹V. A. M. Brabers, *Handbook of Magnetic Materials* (Elsevier Science B.V., Amsterdam, 1995).
 - ²H. D. Han, H. L. Luo, and Z. Yang, *J. Magn. Magn. Mater.* **161**, 376 (1996).
 - ³C. H. Cunningham, T. Arai, P. C. Yang, M. V. McConnell, J. M. Pauly, and S. M. Connolly, *Magn. Reson. Med.* **53**, 999 (2005).
 - ⁴P. Seneor, A. Fert, J.-L. Maurice, F. Montaigne, F. Petroff, and A. Vaurès, *Appl. Phys. Lett.* **74**, 4017 (1999).
 - ⁵G. Hu and Y. Suzuki, *Phys. Rev. Lett.* **89**, 276601 (2002).
 - ⁶J. M. Hastings and L. M. Corliss, *Rev. Mod. Phys.* **25**, 114 (1953).
 - ⁷E. W. Gorter, *Philips Res. Rep.* **9**, 295 (1954).
 - ⁸K. N. Subramanyam, *J. Phys. C* **4**, 2266 (1971).
 - ⁹D. Carta, M. F. Casula, A. Falqui, D. Loche, G. Mountjoy, C. Sangregorio, and A. Corrias, *J. Phys. Chem. C* **113**, 8606 (2009).
 - ¹⁰V. G. Hadjiev, M. N. Iliev, and I. V. Vergilov, *J. Phys. C* **21**, L199 (1988).
 - ¹¹M. Iliev, G. Güntherodt, and H. Pink, *Solid State Commun.* **27**, 863 (1978).
 - ¹²O. N. Shebanova and P. Lazor, *J. Solid State Chem.* **174**, 424 (2003).
 - ¹³P. R. Graves, C. Johnston, and J. J. Campaniello, *Mater. Res. Bull.* **23**, 1651 (1988).
 - ¹⁴Z. H. Zhou, J. M. Xue, J. Wang, H. S. O. Chan, T. Yu, and Z. X. Shen, *J. Appl. Phys.* **91**, 6015 (2002).
 - ¹⁵M. A. Laguna-Bercero, M. L. Sanjuán, and R. I. Merino, *J. Phys.: Condens. Matter* **19**, 186217 (2007).
 - ¹⁶W. H. Wang and X. Ren, *J. Cryst. Growth* **289**, 605 (2006).
 - ¹⁷M. N. Iliev (unpublished).
 - ¹⁸M. N. Iliev, M. V. Abrashev, V. N. Popov, and V. G. Hadjiev, *Phys. Rev. B* **67**, 212301 (2003).
 - ¹⁹C. Haas, *J. Phys. Chem. Solids* **26**, 1225 (1965).
 - ²⁰G. D. Gale, *J. Chem. Soc., Faraday Trans.* **93**, 629 (1997).
 - ²¹G. V. Lewis and C. R. A. Catlow, *J. Phys. C* **18**, 1149 (1985).